

*Supplementary Information for*

**Novel High-Efficiency Crystalline-Si-Based Compound  
Heterojunction Solar Cells: HCT (Heterojunction with Compound  
Thin-layer)**

Yiming Liu<sup>1,2</sup>, Yun Sun<sup>1\*</sup>, Wei Liu<sup>1</sup>, Jianghong Yao<sup>2</sup>

<sup>1</sup>*Institute of Photo-electronic Thin Film Devices and Technology, Nankai University,  
Tianjin 300071, China*

<sup>2</sup>*Department of Physics, Nankai University, Tianjin 300071, China*

## S1. Contents

This document contains supplementary information for the paper entitled “Novel High-Efficiency c-Si Based Compound Heterojunction Solar Cells: HCT (Heterojunction with Compound Thin-layer)”. Section S2 details the carrier transport mechanism at the heterojunction interface. Section S3 presents the modeling input GUI in the solar cell simulation program, wxAMPS, and describes the modeling setup of c-Si surface recombination. Section S4 contains the material parameters used in the simulation.

## S2. Carrier Interface Transport

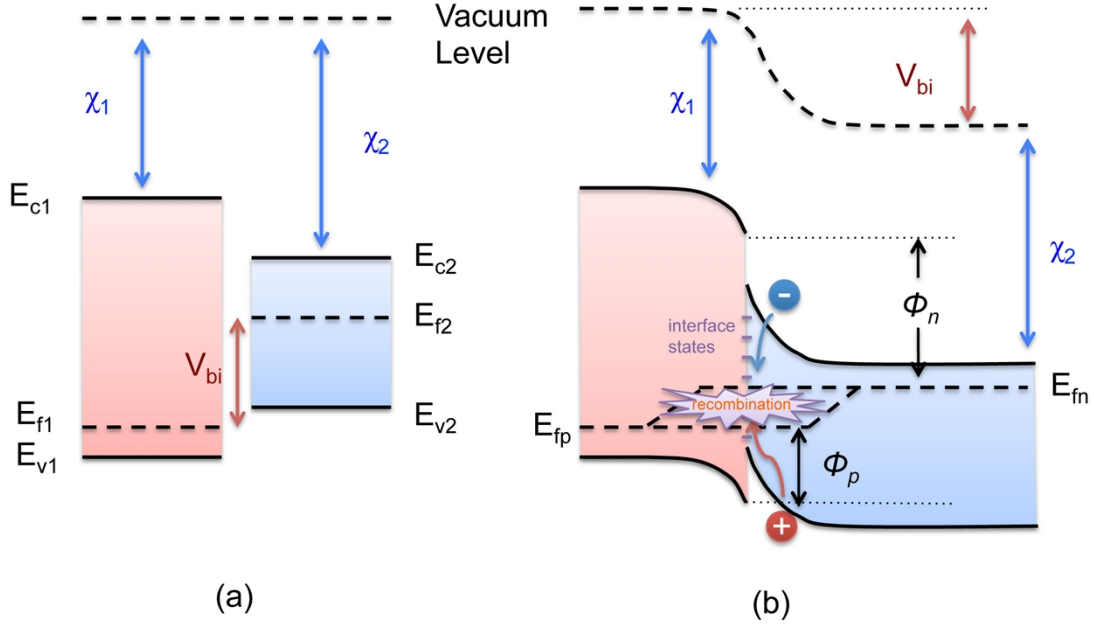


**Figure S1.** **a.** a hetero-interface energy band diagram between two different semiconductors before contact. **b.** a hetero-interface energy band diagram between two different semiconductors after contact, in this case heterojunction has been formed.  $\chi$  is electron affinity,  $E_c$  stands for conduction band and  $E_v$  stands for valence band,  $E_f$  is the Fermi energy level,  $E_{fn}$ ,  $E_{fp}$  stand for quasi-Fermi levels for electrons and holes of both materials, respectively.  $V_{bi}$  denotes the built-in potential at heterojunction, and  $\Phi_n$ ,  $\Phi_p$  represent the height of blocking barriers for electron and holes, respectively. The subscripts 1, 2 indicate the parameter attributed to material 1 and material 2, respectively.

### S2.1 Interface Barrier

The recombination rate  $R$  which considers tunneling-enhanced effects can be estimated as<sup>1</sup>:

$$R = \frac{N_t V_{th} \sigma_n (1 + \Gamma_n) (1 + \Gamma_p) \sigma_p (np - n_i^2)}{\sigma_n (1 + \Gamma_n) (n + n_t) + \sigma_p (1 + \Gamma_p) (p + p_t)} \quad (\text{Eq. S1})$$

where  $N_t$  is the defect density,  $V_{th}$  is the thermal velocity,  $n$ ,  $p$  are the concentrations of electrons and holes,  $n_i$  is the intrinsic carrier density, and  $\sigma_n$  and  $\sigma_p$  are the capture cross-section for electrons and holes, respectively.  $\Gamma_n$  and  $\Gamma_p$  are field-driven tunneling functions that account for trap-assisted tunneling effects. In the energy band structure of hetero-interface shown in **Fig. S1(b)**, the type of the interface has been reversed, and electron is the minority carrier at the interface, which means  $n \ll p$ . In this case, Eq. S1 can be reduced to:

$$R \approx N_t V_{th} \sigma_n (1 + \Gamma_n) n \quad (\text{Eq. S2})$$

As seen in Eq. S2, the recombination rate at the interface mainly depends on the minority carrier density. And the amount of electrons arrived at the hetero-interface can be given by using Boltzmann distribution<sup>2</sup>:

$$n = N_c e^{-\phi_n/kT} \quad (\text{Eq. S3})$$

where  $N_c$  is the local effective density of states for conduction band. According to the intra-band tunneling model, the electron current at the hetero-interface  $J_{int}$  is described as <sup>3</sup>:

$$J_{int} = A^* T^2 e^{-\phi_n/kT} (e^{-\Delta E_{fn}(int)/kT} - 1)(1 + \delta) \quad (\text{Eq. S4})$$

where  $A^*$  is the Richardson constant for the smaller electron effective mass between two adjacent materials,  $\Delta E_{fn}(int)$  is the quasi-Fermi level difference for electrons at interface, and the intra-band tunneling coefficient  $\delta$ . Similar equations are applied to the interface transportation of holes. As shown in Eq. S3~S4, the electron blocking barrier  $\Phi_n$  exponentially influences the electron density at the interface as well as the electron current across the interface. Therefore, according to Eq. S2 the interface recombination is able to be decreased dramatically by increasing  $\Phi_n$ .

For the majority carrier hole, its current across the heterojunction constitute the main proportion of the interface current. Hence, the blocking barrier  $\Phi_p$  is expected as low as possible so as to allow most of the majority carrier to flow through the interface.

In this research, material 2 is crystalline Si (c-Si), and material 1 is the alternative thin film to amorphous Si (a-Si:H). Based on the discussion above, an ideal material 1 should possess low  $\chi_1$  to reduce  $\Phi_n$ , and thus reduce the interface recombination. Meanwhile, its band gap can not be too large, otherwise it will introduce a high  $\Phi_p$  in valence band, which is detrimental to the current transport the interface, and deteriorates the device performance.

## S2.2 Built-in Potential

The heterojunction built-in potential arises from the work function difference between two adjacent materials before contact. Its value depends on doping levels and energy band structures of two materials, and is evaluated by<sup>2</sup>:

$$V_{bi} = \chi_1 + E_{g1} - kT \ln \frac{N_{v1}}{N_{A1}} - \chi_2 - kT \ln \frac{N_{c2}}{N_{D2}} \quad (\text{Eq. S5})$$

where  $E_g$  is the band gap,  $N_V$  is the effective density of states for valence band, and  $N_A$ ,  $N_D$  are the doping concentrations for holes and electrons, respectively.

In the heterojunction structure shown in **Fig. S1(b)**, material 1 acts as an emitter layer which is heavily doped. In this case,  $N_{A1} \gg N_{D2}$ , and most of the space charge region (SCR) lies in material 2. The electric field in SCR contributes to separating the photo-excited carriers, and generates photovoltaic effects. And the SCR width in material 2,  $d$ , at thermal equilibrium is estimated by<sup>2</sup>:

$$d \approx \sqrt{\frac{2\varepsilon_2 V_{bi}}{qN_{D2}}} \quad (\text{Eq. S6})$$

where  $q$  is the basic electron charge,  $\varepsilon$  is the permittivity. And the maximum of electric field  $E_{max}$  at the hetero-interface is given by:

$$E_{max} = \frac{qN_{D2}d}{2\varepsilon_2} \quad (\text{Eq. S7})$$

According to Eq. S6~S7,  $V_{bi}$  determines the SCR width and the electric field at the heterojunction. The increment of  $V_{bi}$  is beneficial to the photocurrent collection.

### S3. Modeling Input in wxAMPS

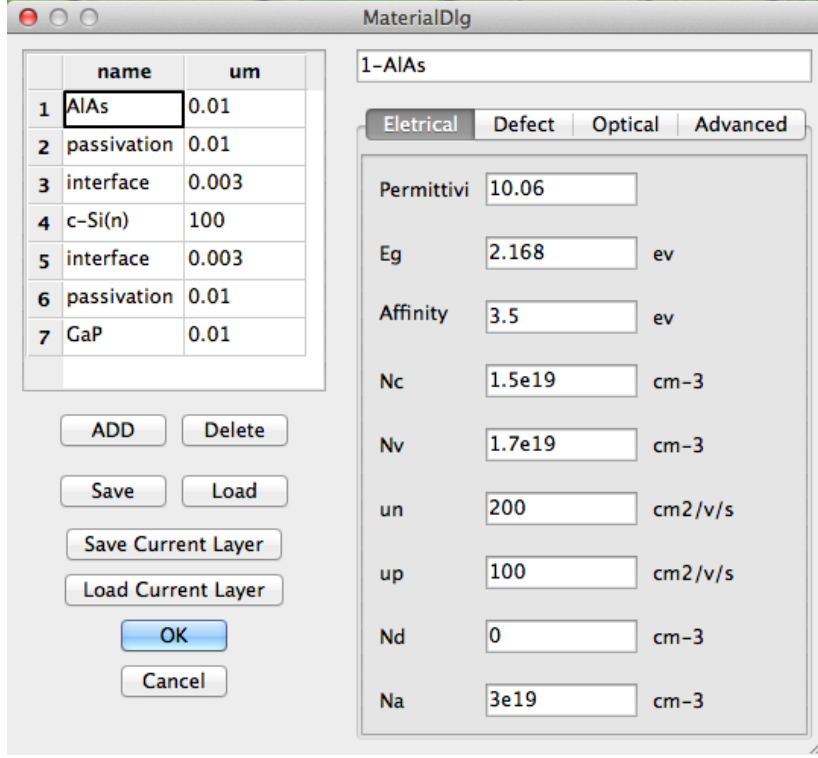


**Figure S2.** Graphical modeling input interface in wxAMPS.

wxAMPS is a numerical solar cell modeling software which considers the trap-assisted tunneling effects and intra-band tunneling mechanism<sup>1,4</sup>. **Figure S2** exhibits its graphical user interface for inputting device structure and material parameters<sup>5</sup>. The device structure of HCT solar cell is displayed on the up-left side of the dialog box.

Due to dangling bonds and lattice disturbance at the c-Si surface, defect states are introduced in the energy band and result in efficiency loss. In the wxAMPS modeling, there are two artificial interface layers on both sides of c-Si, which mimic the c-Si surface recombination. The interface defect density ( $D_{it}$ ) is set as<sup>6</sup>:

$$D_{it} = G_{mg} E_g x_0 \quad (\text{Eq. S8})$$

where  $G_{mg}$  is the density of background mid-gap states,  $x_0$  is the interface layer thickness. More details of interface layers are listed in **Table S2** in the next section. And the interface recombination velocity ( $S$ ) is evaluated by a numerical approach:

$$S_m = \frac{\int R dx}{m} \quad (\text{Eq. S9})$$

where  $R$  is the recombination rate within the interface layer,  $int$  stands for the whole interface layer,  $m$  denotes the concentration of the minority carrier arriving at the c-Si interface, which is  $p$  (hole) for  $n$ -type c-Si substrate, and  $n$  (electron) for  $p$ -type c-Si substrate, respectively. The exact values of  $R$  and  $m$  are obtained from the numerical solution, and the integral of  $R$  across the whole interface layer represents the total interface recombination. This numerical method is more accurate than using the empirical equation:  $S=w/2\tau_{eff}$  ( $w$  is the c-Si bulk thickness,  $\tau_{eff}$  is the effective minority carrier lifetime which can be measured), in which the c-Si bulk recombination is assumed zero, and thus the surface recombination velocity is overestimated.

The surface recombination velocity is an important parameter for assessing the surface passivation and the interface quality. The lower the surface recombination, the better the whole device efficiency. For the world record HIT solar cell, this value is smaller than 2 cm/s<sup>7</sup>.

S4. Parameters Used in the wxAMPS Simulation<sup>6,8-10</sup>

Table S1. Material Electrical Parameters

	c-Si	AlAs	GaAs	GaP	ZnS	a-Si (baseline)
Thickness (μm)	100	10	10	10	10	p, n: 10 i: 3
Band gap (eV)	1.12	2.168	1.42	2.26	3.68	1.72
Electron affinity (eV)	4.01	3.5	4.07	3.8	3.9	3.8
Dielectric constant	11.9	10.1	13.1	11.1	8.9	11.9
Effective conduction band density (cm <sup>-3</sup> )	2.8x10 <sup>19</sup>	1.5x10 <sup>19</sup>	4.4 x10 <sup>17</sup>	1.9x10 <sup>19</sup>	2.2x10 <sup>18</sup>	2.5x10 <sup>20</sup>
Effective valence band density (cm <sup>-3</sup> )	1.0x10 <sup>19</sup>	1.7x10 <sup>19</sup>	7.7 x10 <sup>18</sup>	1.2x10 <sup>19</sup>	1.8x10 <sup>19</sup>	2.5x10 <sup>20</sup>
Electron mobility (cm <sup>2</sup> /Vs)	1350	200	8500	110	100	1
Hole mobility (cm <sup>2</sup> /Vs)	450	100	400	75	25	0.1
Doping concentration (cm <sup>-3</sup> )	p, n: 3x10 <sup>15</sup>	p: 3x10 <sup>19</sup>	n: 1x10 <sup>19</sup>	n: 1x10 <sup>19</sup>	n: 1x10 <sup>19</sup>	p: 3x10 <sup>19</sup> n: 1x10 <sup>19</sup> i: 0
Defect Parameters						
Gaussian density (cm <sup>-3</sup> )		1x10 <sup>15</sup> ~ 2 x10 <sup>18</sup>				p, n: 2 x10 <sup>18</sup> i: 2 x10 <sup>16</sup>
Gaussian peak energy level, donor, acceptor (eV) <sup>a</sup>		mid-gap, mid-gap				1.22, 1.02
Standard deviation (eV)		0.23				
Capture cross-section for acceptor state, e,h (cm <sup>-2</sup> )		1x10 <sup>-15</sup> , 1x10 <sup>-14</sup>				
Capture Cross-section for donor state, e,h (cm <sup>-2</sup> )		1x10 <sup>-14</sup> , 1x10 <sup>-15</sup>				
Band tail density of states (cm <sup>-3</sup> )	1x10 <sup>14</sup>	2x10 <sup>21</sup>				
Characteristic energy, CB, VB (eV) <sup>b</sup>	0.01, 0.01	0.03, 0.06				
Capture cross-section for CB, e,h (cm <sup>-2</sup> )	1x10 <sup>-17</sup> , 1x10 <sup>-15</sup>	1x10 <sup>-17</sup> , 1x10 <sup>-15</sup>				
Capture Cross-section for VB, e,h (cm <sup>-2</sup> )	1x10 <sup>-15</sup> , 1x10 <sup>-17</sup>	1x10 <sup>-15</sup> , 1x10 <sup>-17</sup>				
Midgap density	1x10 <sup>11</sup>					
Switch-over energy	0.56					
Capture cross-section for acceptor state, e,h (cm <sup>-2</sup> )	1x10 <sup>-17</sup> , 1x10 <sup>-15</sup>					
Capture Cross-section for donor state, e,h (cm <sup>-2</sup> )	1x10 <sup>-15</sup> , 1x10 <sup>-17</sup>					

<sup>a</sup>: positive down from the conduction band

<sup>b</sup>: CB denotes conduction band tail, VB denotes valence band tail

Table S2. Interface Defect Parameters<sup>6</sup>

Total interface density of states, $D_{it}$ (cm <sup>-2</sup> )	2.18x10 <sup>5</sup> ~2.18x10 <sup>13</sup>
Thickness, $x_0$ (μm)	0.003
Band tail density of states (cm <sup>-3</sup> )	1x10 <sup>9</sup>
Characteristic energy, CB, VB <sup>b</sup> (eV)	0.01, 0.01
Capture cross-section for CB, e,h (cm <sup>-2</sup> )	1x10 <sup>-17</sup> , 1x10 <sup>-15</sup>
Capture Cross-section for VB, e,h (cm <sup>-2</sup> )	1x10 <sup>-15</sup> , 1x10 <sup>-17</sup>
Midgap density, $G_{mg}$ (cm <sup>-3</sup> )	6.5x10 <sup>11</sup> ~6.5x10 <sup>19</sup>
Switch-over energy (eV)	0.56
Capture cross-section for acceptor state, e,h (cm <sup>-2</sup> )	1x10 <sup>-17</sup> , 1x10 <sup>-15</sup>
Capture Cross-section for donor state, e,h (cm <sup>-2</sup> )	1x10 <sup>-15</sup> , 1x10 <sup>-17</sup>

Note: other electrical parameters of the interface layer are the same as those of c-Si

## S5. References

1. Liu, Y., Sun, Y. & Rockett, A. A new simulation software of solar cells — wxAMPS. *Sol. Energy Mater. Sol. Cells* (2012). doi:10.1016/j.solmat.2011.10.010
2. Fonash, S. *Solar Cell Device Physics*. (Academic Press, 2010).
3. Liu, Y., Sun, Y. & Rockett, A. An improved algorithm for solving equations for intra-band tunneling current in heterojunction solar cells. *Thin Solid Films* (2012). doi:10.1016/j.tsf.2012.03.012
4. Liu, Y., Heinzl, D. & Rockett, A. A new solar cell simulator: WxAMPS. *2011 37th IEEE Photovolt. Spec. Conf.* 002753–002756 (2011). doi:10.1109/PVSC.2011.6186517
5. Liu, Y., Heinzl, D. & Rockett, A. A revised version of the AMPS simulation code. ... *Spec. Conf. (PVSC)*, ... 001943–001947 (2010). doi:10.1109/PVSC.2010.5616225
6. Hernández-Como, N. & Morales-Acevedo, A. Simulation of hetero-junction silicon solar cells with AMPS-1D. *Sol. Energy Mater. Sol. Cells* **94**, 62–67 (2010).
7. Taguchi, M. *et al.* 24.7% Record Efficiency HIT Solar Cell on Thin Silicon Wafer. *IEEE J. Photovoltaics* (2013).
8. Vurgaftman, I., Meyer, J. R. & Ram-Mohan, L. R. Band parameters for III–V compound semiconductors and their alloys. *J. Appl. Phys.* **89**, 5815 (2001).
9. Schubert, E. F. Room temperature properties of semiconductors: III–V phosphides Quantity. <http://homepages.rpi.edu/~schubert/Educational-resources/Materials-Semiconductors-III-V-phosphides.pdf> **1**, 1
10. D W Palmer. Semiconductors Information. [www.semiconductors.co.uk](http://www.semiconductors.co.uk) (2006).